Real Space Analysis of the Structural Evolution of a Polymer Blend via Spinodal Decomposition

Alexander E. Ribbe and Takeji Hashimoto*

Department of Polymer Chemistry, Graduate School of Engineering, Kyoto University, Kyoto 606-01, Japan

Received February 25, 1997; Revised Manuscript Received April 18, 1997[⊗]

ABSTRACT: Transmission electron microscopy (TEM) and laser scanning confocal microscopy (LSCM) are used to visualize the morphological evolution during spinodal decomposition (SD) of a binary polymer blend of poly(styrene-*ran*-butadiene) and polybutadiene with near critical composition. The mechanically homogenized samples were exposed to a temperature jump, and the time evolution of the characteristic wavenumber q_m was recorded by time-resolved light scattering. TEM and LSCM micrographs at various stages are also presented to clarify the growing bicontinuous morphology. A real space analysis of the early stage of the spinodal decomposition is presented for the first time. Two-dimensional Fourier transformation was applied to the real space images to obtain information about the characteristic wavenumber, and the results were compared to the predictions obtained by Cahn's linearized theory.

I. Introduction

The demixing process of thermodynamically unstable mixtures of simple fluids, metals, glasses, or polymers is well known as spinodal decomposition (SD).[1] The structural evolution of polymer mixtures during this phase separation process has been studied by using scattering methods, such as light[2−6] and neutron scattering,[7,8] and microscopic methods, such as optical[9−14] and electron microscopy.[15−19] It also has been studied theoretically[20] and numerically with computer simulations.[21−24] For various polymer blends, including the poly(styrene-*ran*-butadiene) (SBR) and polybutadiene (PB) system which we deal with in this work, time-resolved light scattering method (TRLS) has been applied to investigate the kinetics of the SD process.[25−29]

The SD process in *near-critical* mixtures can be divided into (i) early stage, (ii) intermediate stage, and (iii) late stage.[4] In the early stage the time evolution of the concentration fluctuations can be approximated by the linearized theory,[30−32] first proposed by Cahn.[1] The characteristic wavenumber $q_m(t,T)$, which is related to the domain spacing $\Lambda_m(t,T)$,

$$\Lambda_m(t,T) = 2\pi/q_m(t,T) \tag{1}$$

of the dominant mode of the concentration fluctuations at time t and phase-separation temperature T is independent of t. The intensity of the Fourier mode of the fluctuations with wavenumber q, $I(q,t,T)$, grows exponentially with the time. The intermediate stage is characterized by a decrease of $q_m(t,T)$ as well as a further increase of the intensity due to a nonlinear nature in the time evolution of the concentration fluctuations.[33] In the late stage the two phases reach equilibrium composition and the interface between the two phases narrows to equilibrium thickness.[34,35] The domains, however, $\Lambda_m(t,T)$ are still increasing in order to lower the interfacial free energy of the system.

The morphological evolution of near-critical mixtures was the topic of various microscopic investigations,[9−19,36,37] showing generally bicontinuous morphologies with growing domain spacing. However microscopic investigations over a wide time range starting from the onset of the SD, especially in comparison with light scattering investigations performed parallel, are up to now missing.

The main aim of this paper is to present a detailed morphological investigation on the SD of a near-critical mixture of SBR and PB using TEM and laser scanning confocal microscopy (LSCM) of all stages, i.e., early, intermediate, and late stages. Second, we will qualitatively compare the morphologies determined by the real space analysis with those determined by the Fourier space analysis based on TRLS. The experimental results will be compared with the existing theories.

Table 1. Characteristics of the Polymers Used in This Study[a]

	polybutadiene (PB20)	poly(styrene-*ran*-butadiene) (SBR20)
styrene content[c]		20 wt %
M_W[b]	2.23×10^5	1.79×10^5
N_W	4.13×10^3	3.00×10^3
M_W/M_N[b]	1.3	1.2
1,4-cis[c]	23%	17%
1,4-trans[c]	37%	31%
1,2-vinyl[c]	40%	52%

[a] M_W and N_W are the weight-average molecular weight and polymerization index, respectively. [b] Determined by GPC where M_n is the number-average molecular weight. [c] Determined by IR.

II. Experimental Section

A. Sample. The two polymers coded as SBR20 and PB20 have molecular weight and microstructure given in Table 1. The binary mixtures have a near-critical composition of 47 vol % SBR (50/50, wt %/wt %, SBR/PB). The polymers were dissolved in toluene, containing 5 wt % polymer in total. This solution was cast into thin film specimens in Petri dishes, where the solvent was allowed to evaporate over 1 week at 30 °C. The 0.15 mm thick samples were further dried in a high-vacuum oven until no mass loss could be observed.

B. Mechanical Mixing. The two-phase morphology of the as-cast film cannot be brought into single phase state by raising the temperature. Therefore a previously described mechanical mixing process[38,39] called Baker's transformation was applied. The film is folded and pressed between two glass slides until the original thickness is regained. This process is repeated several times until the mixture becomes homogenous. Immediately after the stop of the homogenization process phase separation starts.

C. Transmission Electron Microscopy. The samples used for transmission electron microscopy were obtained by annealing the homogenized samples in a heater block con-

[⊗] Abstract published in *Advance ACS Abstracts,* June 1, 1997.

S0024-9297(97)00258-1 CCC: $14.00

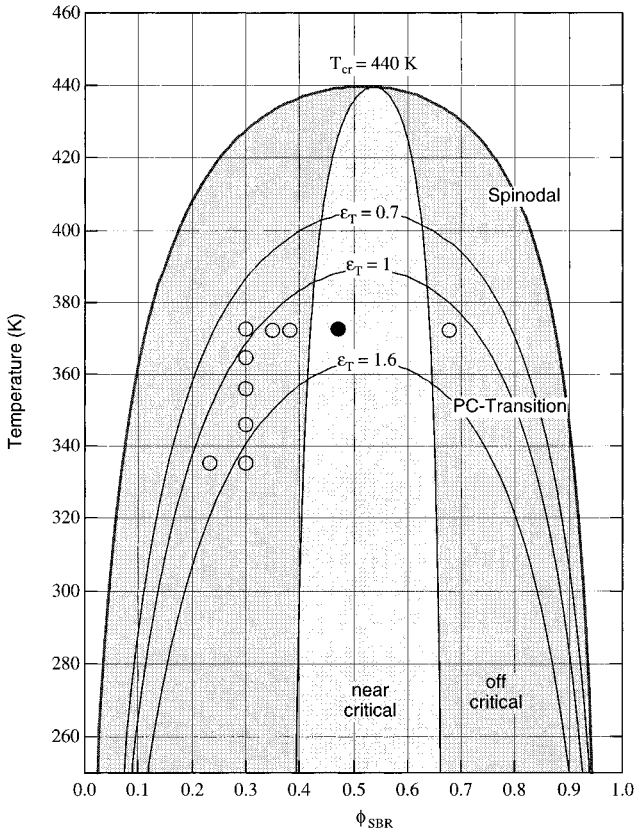

Figure 1. Phase diagram of SBR20/PB20. Included are the near-critical mixture investigated in this study (●) and mixtures with off-critical compositions (○) which will be discussed in a companion paper.[41]

trolled at 100 °C under vacuum. After the respective annealing times, the samples were cooled down in ice water and then in liquid nitrogen. The thus obtained samples were then cut using a low-temperature ultramicrotome Reichert/Nissei Ultracut FC4E equipped with a diamond knife at −100 °C, and the 30−50 nm ultrathin sections were stained with OsO_4 vapor while warming up to room temperature. We used high molecular weight polymers for this examination in order to have a sufficiently slow phase separation. This is to avoid artifacts induced by a further growth of the phase-separating structure during the staining process of the sample as much as possible. A staining for 1−2 min was sufficient enough to obtain good contrast in the TEM. We assume that the staining time is enough to cross-link the sample so that further phase separation is stopped, as the observed morphology on the stained ultrathin sections does not change, even after weeks. The optimum contrast was achieved after a staining time of about 20 min, where the PB is primarily stained by the OsO_4. After a longer staining time both the PB and SBR were stained. A TEM (Hitachi HS600) with 100 kV acceleration voltage was used.

D. Laser Scanning Confocal Microscopy. No special treatment of the sample was required for LSCM. LSCM measurements were done with a LSM 320 (ZEISS) using a He/Ne laser with $\lambda = 632.8$ nm wavelength, and image processing was done with the firm software supplied by Zeiss. The microscope has an excellent spatial resolution along the depth direction because of the following mechanism. The laser beam from the light source is passed through a beam splitter and focused on the sample via the scanner through the tube lens and objective lens. Light reflected or emitted from the focal plane is directed back through the objective lens, the tube lens, the scanner, and the beam splitter. It is then focused on and passed through a pinhole and directed to the detector. The light emanating from other planes cannot pass through the pinhole as it is focused at a place other than the pinhole position and hence is effectively suppressed. As a detector a photomultiplier is used. A detailed description of the apparatus[40] and the image generation[12−14] can be found in the literature. The contrast between the two phases is generated by reflected light[40] at the interface of the two phases and by excess scattering arising from the SBR phase in the SBR/PB mixture (scattering-induced contrast generation).[14]

E. Time Resolved Light Scattering. The TRLS was carried out with a laser with $\lambda = 632.8$ nm wavelength. A detailed description of the apparatus is given elsewhere.[2]

III. Results and Discussion

In the following we will first discuss the phase diagram of the SBR20/PB20 mixture (section A). TRLS and the structural evolution as observed by TEM and LSCM will be presented in sections B and C, respectively. Lastly, we present a 2D-FFT analysis of the TEM images of the early stage (section D), the results of which will be compared to the data obtained from the light scattering by application of Cahn's linearized theory.

A. Phase Diagram. The temperature dependence of the Flory−Huggins (FH) interaction parameter χ between SBR and PB at a given composition (50 vol % SBR) was determined from the cloud points T_{cl} measured for the following two blends of SBR and PB at the same blending composition and the same microstructure as SBR20 and PB20 but with different molecular weight, based on the FH theory. The two blends used were SBR5/PB5 ($N_{W,SBR} = 820$, $N_{W,PB} = 900$) having $T_{cl} = 40$ °C and SBR5/PB10 ($N_{W,SBR} = 820$, $N_{W,PB} = 1650$) having $T_{cl} = 70$ °C, with $N_{W,SBR}$ and $N_{W,PB}$ being the weight-average polymerization indices of the respective polymers. SBR5 and SBR20 have the identical composition of styrene units. In the context of the FH theory the χ-value at the spinodal point, χ_s, is given by

$$\chi_s = \frac{\nu_o}{2}\left(\frac{1}{N_{W,SBR}\phi_{SBR}\nu_{SBR}} + \frac{1}{N_{W,PB}\phi_{PB}\nu_{PB}}\right) \qquad (2)$$

where ϕ_{SBR} and ϕ_{PB} are the volume fractions of SBR and PB in the mixture and ν_{SBR} and ν_{PB} are the segment volumes. Using a volume fraction $\phi_{SBR} = \phi_{PB} = 0.5$, a molar volume $\nu_{SBR} = 72$ cm^3/mol, $\nu_{PB} = 65$ cm^3/mol, and an averaged molar volume $\nu_0 = (\phi_{SBR}/\nu_{SBR} + \phi_{PB}/\nu_{PB})^{-1} = 68$ cm^3/mol, we can estimate χ_s for the two blends from eq 2. In order to determine χ as a function of T, we assume that (i) $T_{cl} \cong T_b \cong T_s$ (T_s being the temperature at spinodal point and T_b the temperature at binodal point) and (ii) the temperature dependence of χ is given by

$$\chi = a + b/T \qquad (3)$$

The former assumption (i) is reasonable for critical composition, and the latter (ii) has been generally accepted in literature. Since the relations between χ_s ($=a + b/T_s$) and T_s ($=T_{cl}$) are known for the two blends, we obtain two sets of equations, from which we can solve the unknown constants a and b in eq 3. The result is given by

$$\chi = -3.7237 \times 10^{-3} + 1.891/T \qquad (4)$$

Using the values of $N_{W,SBR} = 3.00 \times 10^3$ and $N_{W,PB} = 4.13 \times 10^3$ for the SBR20/PB20 mixture, we obtain a critical temperature of $T_{cr} = 167$ °C. Figure 1 shows the spinodal line of SBR20/PB20 calculated under the assumption that χ is independent of the composition. The direct measurement of the cloud points is hardly possible as the SBR/PB mixtures undergo thermal cross-linking at $T \geq 403$ K. Even adding antioxidant does

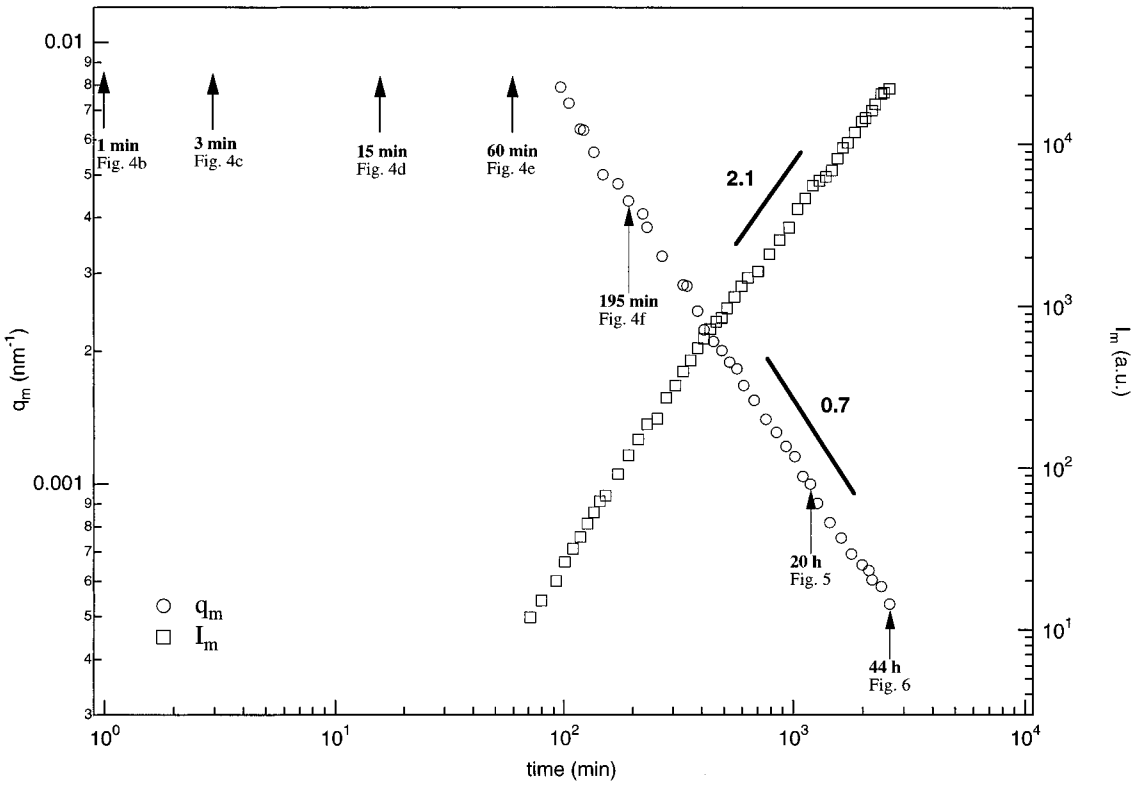

Figure 2. Time evolution of the characteristic wavenumber $q_m(t)$ and the intensity $I_m(t)$ at $q_m(t)$ for the near-critical (47 vol % SBR) mixture as measured by TRLS. The points where the real space data shown in Figures 4−6 were taken are also included in this figure.

not suppress the cross-linking over the long time period required for a reasonable determination of the cloud points.

The driving force for the spinodal decomposition, i.e., quench depth, ϵ_T, is given by

$$\epsilon_T = \frac{\chi(T) - \chi_s}{\chi_s} \tag{5}$$

For $\epsilon_T < 1$ the phase separation takes place at a shallow quench or a weak segregation regime. If $\epsilon_T \geq 1$ it occurs at a deep quench or a strong segregation regime. The points where ϵ_T becomes 0.7, 1, and 1.6 as a function of ϕ_{SBR} are also included in Figure 1.

The phase diagram also includes, besides the compositions of the sample investigated in this paper (●), some further samples with off-critical composition (○) which will be discussed in a forthcoming paper.[41] The border between the off- and near-critical regimes, i.e., the regimes where percolation-to-cluster transition does or does not occur, is only qualitatively assessed from the time evolution of the domain structure for different samples with different compositions during the phase separation process. In this paper we only present the sample with near-critical composition annealed at a temperature of 100 °C. Further investigations on an off-critical mixture by a systematical change of the annealing temperature and composition are described in a companion paper.[41]

B. Structural Evolution during SD As Observed by TRLS. The time evolution of the "characteristic wavenumber" $q_m(t,T)$, i.e., the wavenumber of the Fourier modes of the concentration fluctuations having maximum intensity, and the intensity maximum $I_m(t,T)$ of the near-critical mixture (47 vol % SBR) at 100 °C is shown in Figure 2. As reported previously for similar polymer systems,[27,28] near-critical mixtures show a growing domain spacing until our measurements reach the resolution limit (small angle limit) of the scattering apparatus. With the light scattering method we cannot observe the time evolution of $q_m(t,T)$ from the onset of the demixing up to about 1 h in the case of the chosen temperature of 100 °C, simply because the value q_m becomes larger than the large q-limit covered by our apparatus in this time period.

As seen in Figure 2, the *near-critical* mixture shows a decreasing $q_m(t,T)$ and increasing $I_m(t,T)$ during the observable time window. The time evolution of $q_m(t,T)$ and $I_m(t,T)$ are described by

$$q_m(t,T) \sim t^{-\alpha} \tag{6}$$

and

$$I_m(t,T) \sim t^{\beta} \tag{7}$$

In the intermediate stage a relation of $\beta > 3\alpha$ is observed.[42] The late stage is reached when $\beta = 3\alpha$. In the late stage the two phases attain equilibrium compositions, and a self-similar growth of the structure can be observed. The scaled structure factors of the mixture, obtained by using the previously described scaling laws[43,44] for spinodal decomposition, are given in Figure 3. As mentioned above during the early and intermediate stages $\beta > 3\alpha$ and the scattering patterns cannot be scaled by the described scaling law.[43,44] This means that the scaled structure factors during these two stages are not superimposable as in the late stage. As the observed scaled structure factors have almost the same maximum intensity at $x = 1$ (Figure 3), we can assume that the mixture is in the late stage in the time domain of our TRLS observations. Therefore we expect the crossover time t_{cr} for this mixture to be equal to or smaller than 90 min. We observe that the exponents β and α are 2.1 and 0.7, respectively, which stays constant over the whole observation period. The slopes were well estab-

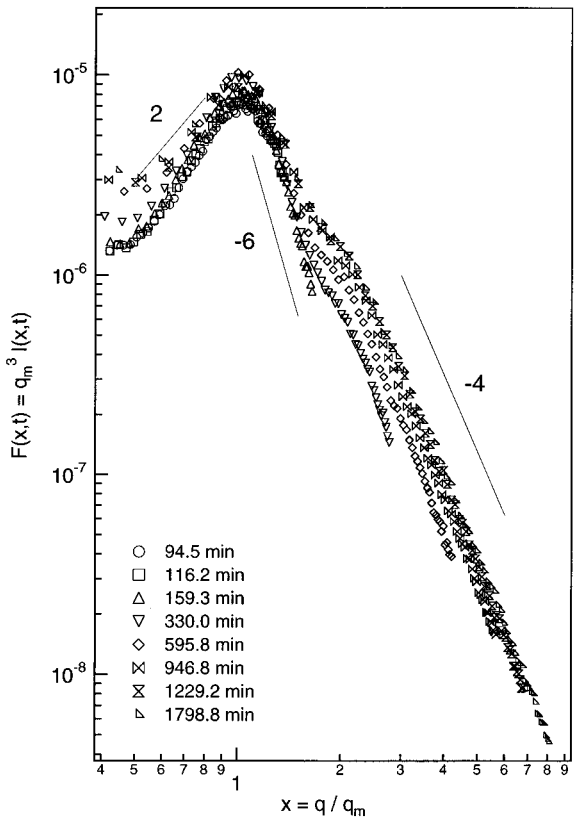

Figure 3. Scaled structure factor obtained for the scattering profiles obtained by TRLS of the near-critical mixture (47 vol % SBR) annealed at 100 °C. At times before 90 min the intensity maximum was not clearly determinable, because q_m exists outside of our q-window.

lished for dynamically growing bicontinuous morphologies of near-critical polymer mixtures with hydrodynamic interactions.[42,45] We should comment on the fact that $F(x,t)$ near $x \cong 1$ ($x \leq 2$) is universal with t but $F(x,t)$ at $x > 2$ increases with t. The latter is caused by a decreasing relative interfacial thickness t_I/Λ_m,[34,35] where t_I is the characteristic interface width. In other words, we need at least two length scales, Λ_m and t_I, in order to characterize the time evolution of the structures over such a large length scale as shown in Figure 3.

C. Morphological Evolution As Observed by TEM and LSCM. In Figure 4 we see the transmission electron micrographs of the polymer blend after (a) 30 folding steps, which is supposed to be the homogenous state (see section III E later), and annealing at 100 °C for (b) 1, (c) 3, (d) 15, (e) 60, and (f) 195 min. The LSCM micrographs after 20 and 44 h of annealing are given in Figures 5 and 6, respectively.

The micrograph of the homogenized sample (Figure 4a) shows a very fine structure with poor contrast. This structure is probably caused by the phase separation induced while preparing the sample for the TEM observations, i.e., during cooling and staining time of the homogenized sample. Although the phase separation of the system is very slow at room temperature, it is not possible to obtain an image of the homogenous state. A more detailed discussion is given in a different paper, which describes the structural change during the applied mixing process.[39]

Starting from very early times after the temperature jump to 100 °C, we observe a bicontinuous structure with an obviously growing domain spacing. The domain spacing of this bicontinuous morphology keeps increasing as can be seen in Figures 4b−f, 5a, and 5b. The determination of the crossover time from the early to the intermediate stage and that from the intermediate to the late stage is difficult from the TEM results. A detailed discussion of the early stage will be given in section III D. According to the theory of SD, the crossover from the intermediate to the late stage is defined by a criterion whether or not the equilibrium composition is attained in the two phases. An influence of the composition fluctuations on the contrast of the TEM images in the expected time range of 10−195 min, however, is hard to quantitatively analyze, partly due to the staining method and the three-dimensional nature of the bicontinuously phase-separating domains. The contrast variation on the TEM images is caused by an overlap of the two phases in the thin slice in the z-direction, i.e., parallel to the incident beam, where the shape of the structure, which is expected to form a hyperbolic interface with a negative Gaussian curvature, determines the observed contrast.[12,36,37,46]

The structure seen on the TEM image in Figure 4e after 60 min of annealing can easily be identified as a 'spongelike' bicontinuous morphology.[37] The structures, however, grow very rapidly. The morphology observed by TEM after 195 min still looks interconnected (Figure 4f). The TEM investigations, however, are limited to a sample thickness of about 50 nm. With time the domain spacing reaches a multiple of this slice thickness, and we can only observe a very thin slice of the space-filling three-dimensional structure. For structures with larger domain spacing, we used LSCM, with which we can identify the morphology where the TEM fails.

Figures 5 and 6 are the result of a three-dimensional reconstruction of 30 slices with focal depths of 600 and 800 nm, respectively. The images in part a give an overall view through the whole depth of 15 μm, i.e., thickness of the 3D-stack composed of a series of sliced images. Parts b1,2 and c1,2 show the slices in the y,z-plane (perpendicular to the x-axis) and x,z-plane (perpendicular to the y-axis) along the blue (b1, c1) and white (b2, c2) lines marked in part a, respectively. The bright phase corresponds to the SBR-rich phase and the dark one to the PB-rich phase.[14] The brightest structure units in Figures 5 and 6 correspond to SBR structure units close to the surface of the depicted sample cell. The color change from white to yellow, orange, red, and purple indicates increasing distance from the surface in this sample cell along the depth direction of the local structure.

The images give us a detailed insight into the features of the spongelike bicontinuous structure which shows tripodlike structure units in many places. For better identification on the images, we indicated two interconnecting tubelike domains of SBR parallel to the x,y-plane by green or red arrows at the same locations in the three different views (a, b2, c2 and a, b1, c2) in space in Figure 6, respectively. The tubelike domains tend to be broken with further elapse of time.

Four selected slices with a distance of 1 μm along the depth direction leading to Figure 6 are shown in Figure 7. The continuity of the two phases is obvious in the x,y-plane. An arrow (a) in Figure 7 locates a part of the SBR domain which interconnects the neighboring SBR domains. The domain is not visible on the first and forth slice but appears on the second and third one. From the slices we can see how the structure is composed of a combination of tripodlike elements which finally form the three-dimensional network. The interfaces, separating the two phases, show a hyperbolic characteristic having a negative Gaussian curvature in most of the places. A much more detailed description

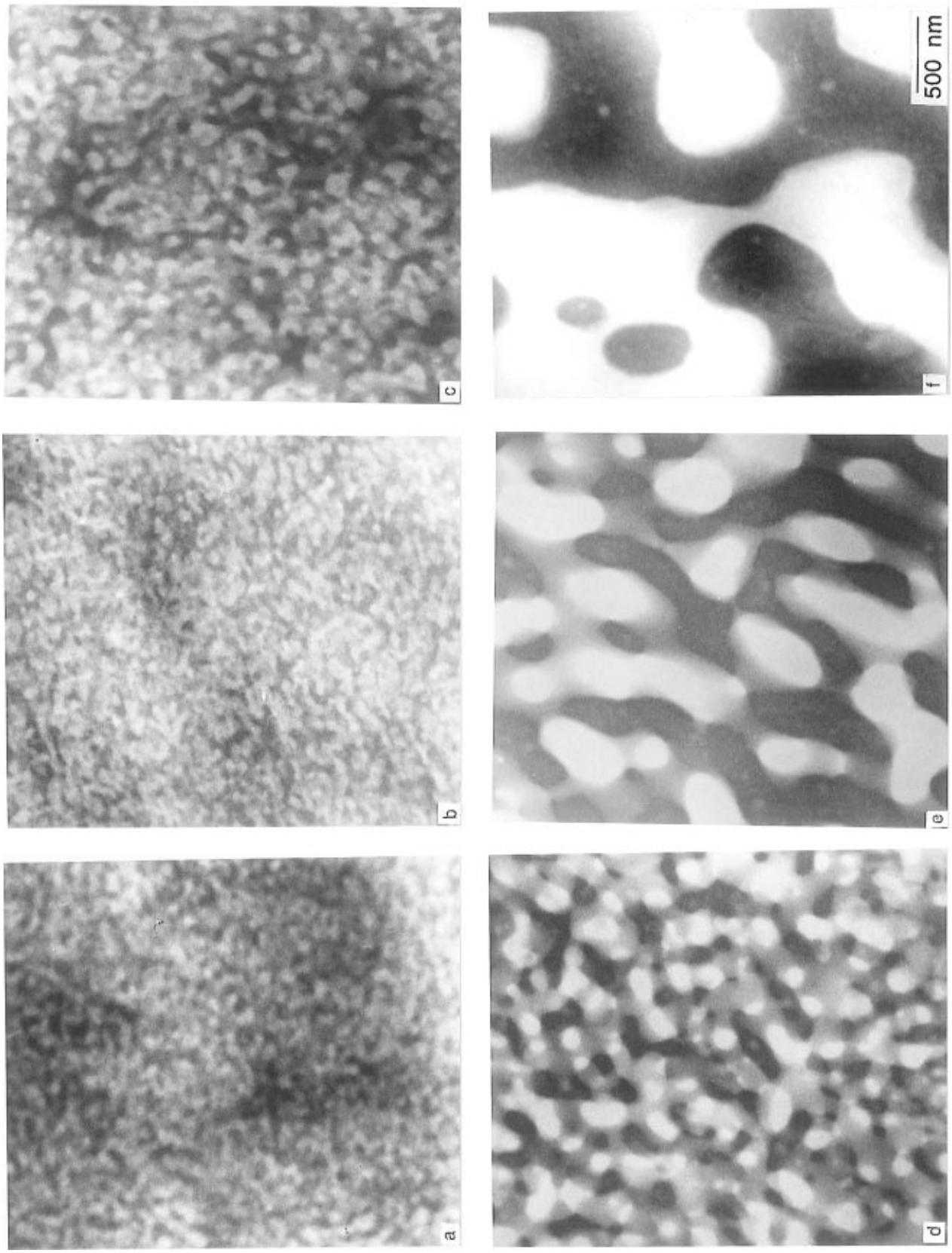

Figure 4. Transmission electron micrographs showing the time evolution of the near critical mixture (47 vol % SBR), first homogenized (a) (after 30 folding steps) and afterward annealed for (b) 1, (c) 3, (d) 15, (e) 60, and (f) 195min at 100 °C. The dark phase corresponds PB-rich phase selectively stained by OsO_4.

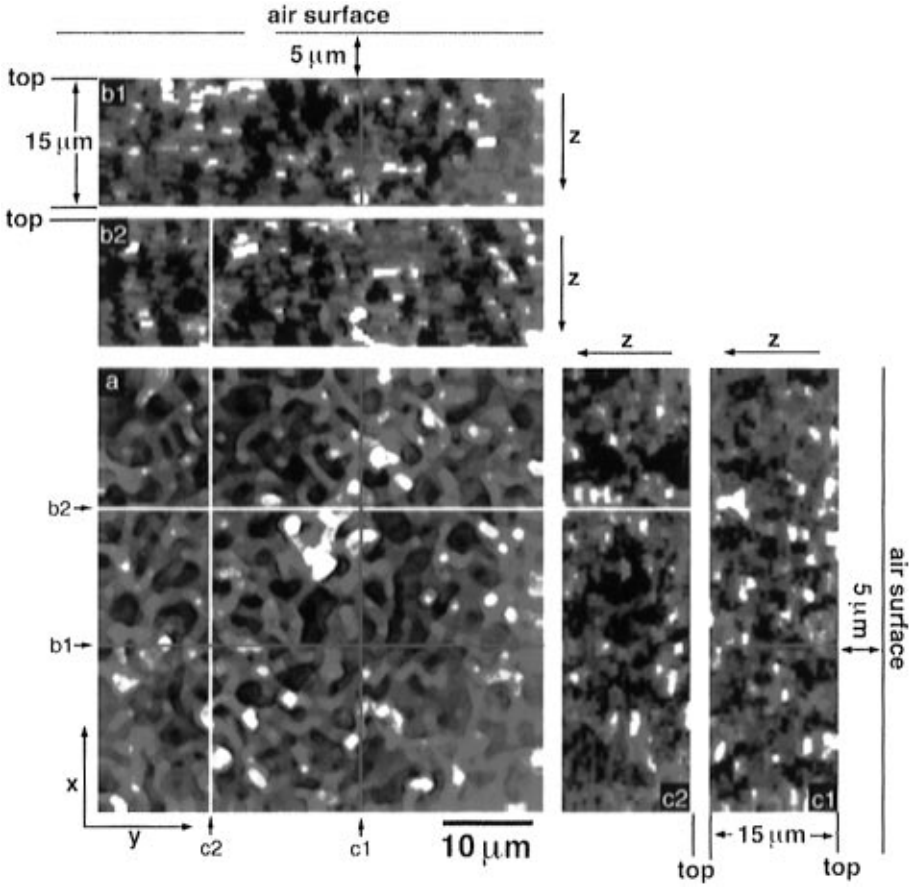

Figure 5. 3D-Reconstruction from 30 LSCM slices with a distance of 500 nm along the depth direction (part a) of the near-critical mixture (47 vol % SBR) annealed for 20 h at 100 °C after homogenization. The blue (b1, c1) or white (b2, c2) lines show the cutting direction where the images in the *y*,*z*-plane (b1,2) and *x*,*z*-plane (c1,2) were obtained. The colored areas correspond to SBR-rich phase. The color change from white to yellow, orange, and red indicates increasing distance from the surface in this sample cell along the depth direction of the local structure.

of the image acquisition and processing for the generation of the depicted images is given elsewhere[12−14,46] and shall not be the topic of this paper. Using a SBR/PB blend of polymers with polymers of the same microstructure but lower molecular weight, it could be shown that the domain spacing of the bicontinuous morphology keeps on growing even after 5 days (7200 min) at 100 °C without undergoing PC transition.[47]

D. Structural Evolution during the Early Stage of SD. As mentioned, the early stage of the SD may be described by Cahn's linearized theory[1] and was applied for polymer systems.[2,3,25,26] According to the theory, which was originally developed for small molecules, the wavenumber for the dominant mode of the concentration fluctuations $q_m(t)$ is independent of the time t and defined hereafter as $q_m(0) \equiv q_m(t=0)$. The Cahn−Hilliard−Cook theory[1,48,49] describing the early stage of SD predicts the time evolution of the scattered intensity, $I(q,t)$ by

$$I(q,t) = I_T(q) + [I(q,t=0) - I_T(q)] \exp[2R(q)t] \quad (8)$$

where $I_T(q)$ is the virtual structure factor[32,49−51] describing the effect of the thermal noise on $I(q,t)$ and $R(q)$ is the growth rate of the Fourier component of the concentration fluctuations with wavenumber q. In the case of deep quench and at $q < q_c$ where q_c is the critical wavenumber satisfying $R(q=q_c) = 0$,

$$|I_T(q)| \ll I(q,t=0) \quad (9)$$

so that $|I_T(q)|$ does not significantly affect $I(q,t)$. In this case we expect an exponential growth

$$I(q,t) = I(q,t=0) \exp[2R(q)t] \quad (10a)$$

$$R(q) = q^2 D_{app}[1 - q^2/2q_m^2(0)] \quad (10b)$$

where D_{app} is the mutual diffusivity. D_{app} and $q_m(0)$ are measurable quantities from the plot $R(q)/q^2$ vs q^2, i.e.,

$$D_{app} = \lim_{q \to 0} [R(q)/q^2] \quad (11a)$$

$$q_m(0) = \left[\frac{1}{2} \lim_{R/q^2 \to 0} q^2\right]^{1/2} \quad (11b)$$

The characteristic time of the blend, $t_c(T)$, at a given temperature T is given in terms of temperature dependent D_{app} and $q_m(0)$, i.e., $D_{app}(T)$ and $q_m(0,T)$:

$$t_c(T)^{-1} = [q_m(0,T)]^2 D_{app}(T) \quad (12)$$

The time evolution of the light scattering intensity $I(q,t)$ at 100 °C and at selected q-values is given in Figure 8a, and the plot of the growth rate $R(q)$ at various wavenumbers q is given in Figure 8b. We observe a linear behavior in both ln $I(q)$ vs q and $R(q)/q^2$ vs q^2 as the theory predicts. From Figure 8b we can determine D_{app}, t_c, and $q_m(0)$ to be 10.97 nm^2/s, 1272 s, and 8.46 × 10^{-3} nm^{-1}, respectively.

As our TRLS method can cover a q-range up to $q \cong 10 \times 10^{-3}$ nm^{-1}, no investigations on the time evolution of Fourier modes of structures with q higher than 10×10^{-3} nm^{-1} have been attained for this mixture yet. Besides there are no real time or in-situ experiments

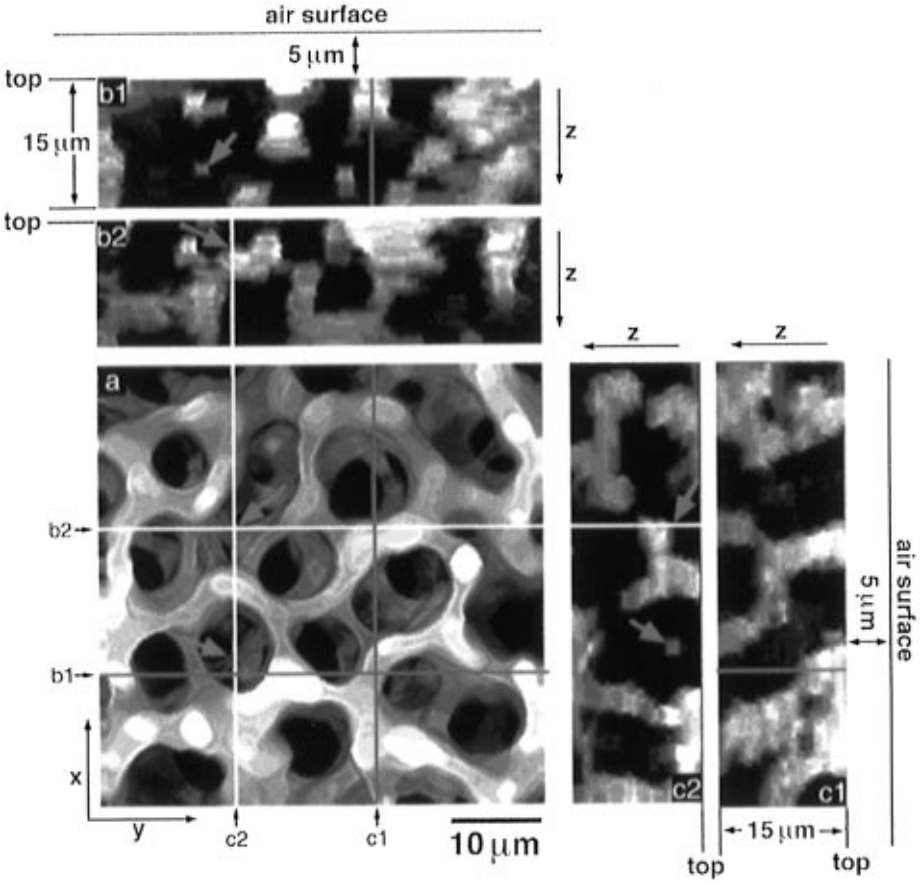

Figure 6. 3D-Reconstruction from 30 LSCM slices with a distance of 500 nm along the depth direction (part a) of the near-critical mixture (47 vol % SBR) annealed for 44 h at 100 °C after homogenization. The blue (b1, c1) or white (b2, c2) lines show the cutting direction where the images in the *y*,*z*-plane (b1,2) and *x*,*z*-plane (c1,2) were obtained. The colored areas correspond to SBR-rich phase. The color change from white to yellow, orange, red, and purple indicates increasing distance from the surface in this sample cell along the depth direction of the local structure.

available for this system which elucidate the evolution of the concentration fluctuations covering the higher q-modes ($q > 10\times10^{-3}$ nm^{-1}) in the early stage of SD. The high resolution of the TEM is advantageous to investigate those small structures. The main problem here is the low amplitude and the fast growth of the concentration fluctuations at the early stage. Therefore the sample preparation, especially the fixation of the structures, has to be very quick to obtain good results and not to observe a morphology developed through the sample preparation procedure. In the case presented here we chose rather high molecular weight polymers in order to have a system with slow kinetics, even in the early stage. The blend with T_gs of −60 °C for SBR and −80 °C for PB was rapidly quenched from 100 °C to liquid nitrogen (see section II C) and then ultramicrotomed at −100 °C, so we can be sure that the morphology is not changing during the ultrathin-sectioning procedure. The thin sections were immediately transferred to a container saturated with OsO_4 vapor. Even after staining for 1 min, the samples showed sufficient contrast in the TEM. As the structure in the ultrathin-sectioned film did not change over weeks, we assume that the staining procedure immediately froze the growth of the phase-separating structure.

The TEM images after 1, 3, and 15 min of annealing at 100 °C (Figure 4b−d) show a bicontinuous structure with a growing domain spacing $\Lambda_m(t,T)$. We can obtain the characteristic wavenumber $q_m(t)$ of the contrast fluctuations, which should correspond to the composition fluctuations, by application of 2D Fourier transformation (2D-FFT) (see Appendix A). The power spectra

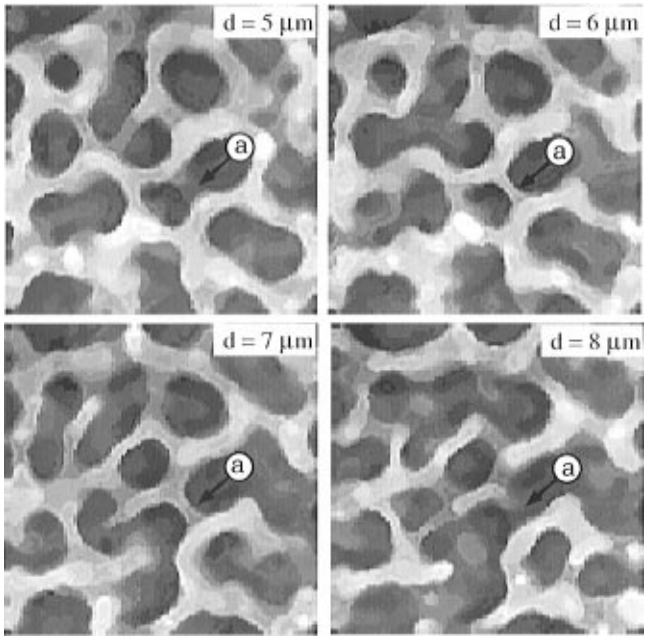

Figure 7. Part of the slice series along the depth direction for the reconstruction of the image in Figure 6. Four slices, starting from the first slice of the series, which originally consisted of 30 slices in 500 nm steps, with a distance of 1 μm are depicted. The focal depth of one slice is 800 nm.

contain nearly same reciprocal space information as a conventional scattering pattern.[53] We estimated q_m^{FFT} from the wavenumber at maximum intensity using a simple Gaussian fit as shown in Figure 9 (see the profile

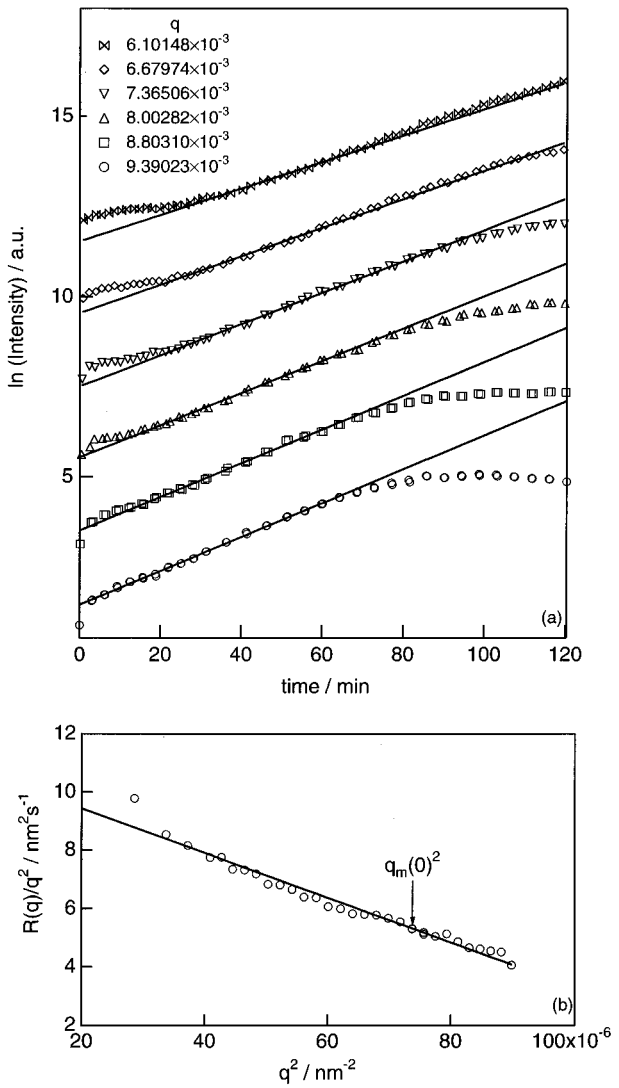

Figure 8. (a) Change of the scattered intensity at various scattering vectors (q) with the time during the early stage of SD for near-critical mixture (47 vol % SBR) at 100 °C. (b) Plot of $R(q)/q^2$ vs q^2.

drawn with a straight line). We can plot the q_m^{FFT} values obtained from FFT together with the data obtained for the time evolution of q_m from the TRLS for the late stage as shown in Figure 10. Further the values for $q_m(0)$ estimated from the 2D-FFT analysis ($q_m(0)^{FFT}$) and from TRLS ($q_m(0)^{TRLS}$), based on the linearized theory, are indicated by dotted lines.

In the context of the mean field theory[30−32] $q_m(0)$ is given by

$$q_m^2(0) = (3/2)\epsilon_T R_g^{-2} \tag{13}$$

where R_g is the radius of gyration which can be calculated by

$$R_g = (Na^2/6)^{1/2} \tag{14}$$

where N ($=\phi_{SBR}N_{SBR} + \phi_{PB}N_{PB}$) is the weight-average polymerization index and a is the statistical segment length. Using $\epsilon_T = [\chi_{100\ °C} - \chi_s]/\chi_s = 1.34$ obtained from the phase diagram in section I ($\chi_s = 5.7403 \times 10^{-4}$, $\chi_{100\ °C} = 1.346 \times 10^{-3}$) and $R_g = 17$ nm calculated from eq 14 ($a_{PB} \cong a_{SBR} \cong a \cong 0.69$ nm[54]), we can determine $q_m(0)^{MF}$ to be 8.34×10^{-2} nm^{-1} corresponding to a domain spacing of $\Lambda_m(0)^{MF} = 75$ nm. This value of $q_m(0)^{MF}$ is close to the value of $q_m(0)^{FFT}$ ($= 4.65 \times 10^{-2}$ nm^{-1}) determined from the TEM-FFT method.

In the TEM images immediately after 1 min of annealing (Figure 4b), it is difficult to find structures that correspond to a periodicity of the concentration fluctuations of $\Lambda_m(0) \cong 2\pi/q_m(0) = 2\pi/8.46 \times 10^{-3}$ nm^{-1} = 740 nm as determined from the TRLS data and the linearized theory described above. Following the time evolution of $q_m(t)$ (Figure 10) toward time → 0, which should correspond to $q_m(0)$ as obtained from FFT [$q_m(0)^{FFT}$], we find $q_m(0)^{FFT} = 4.65 \times 10^{-2}$ nm^{-1} or $\Lambda_m(0)^{FFT} = 2\pi/q_m(0)^{FFT} = 135$ nm, which is more than 5 times smaller than $\Lambda_m(0) = 740$ nm estimated from the linearized theory. The value determined by the mean field theory of $q_m(0)^{MF} = 8.34 \times 10^{-2}$ nm^{-1} or $\Lambda_m(0)^{MF} = 2\pi/q_m(0)^{MF} = 75$ nm, however, indicates a much better agreement with the data obtained from the FFT measurements.

It should be mentioned that the value of $q_m(0) \cong 8.46 \times 10^{-3}$ nm^{-1} estimated from TRLS is close to the high angle limit (65° in air) or high q-limit $\cong 9 \times 10^{-3}$ nm^{-1} of our scattering apparatus, and hence $q_m(0)$ was estimated only from the small q-side of q_m. As the large q-side was missing in our TRLS data, the value of $q_m(0)$ estimated from eq 10b and Figure 8b causes an extrapolation error when using the linearized theory in the described way. Hence $q_m(0)$ as estimated by TRLS might be too low or $\Lambda_m(0)$ too high. This disparity between $q_m(0)^{TRLS}$ and $q_m(0)^{FFT}$ should be further studied by using time-resolved SANS technique which enables determination of $R(q)$ at $q > q_m(0)$.

E. Single-Phase State. The scattering intensity profile of a blend in the single phase state in a small q-limit can be described by the Ornstein−Zernike (OZ) formula:[38,52]

$$I_s(q) = I_s(0)/[1 + q^2\xi^2] \tag{15}$$

with ξ being the correlation length of the thermal concentration fluctuations in the single-phase blend.

As depicted in Figure 11 the experimental results on the scattered intensity $I(q,t=0)$ immediately after the homogenization are in good agreement with the formula of eq 15, suggesting that the scattering is reflecting the thermal concentration fluctuations in the single state. Here the scattered intensity $I(q,t=0)$ was estimated by extrapolating the linear part in the plot of ln $I(q,t)$ vs t to time zero at various q-values. The correlation distance determined from the OZ plot (defined by ξ_{OZ}) is 48 nm, which corresponds to a characteristic wavenumber of $q_{m1} \equiv 1/\xi_{OZ} = 2.1 \times 10^{-2}$ nm^{-1} or $q_{m2} \equiv 2\pi/\xi_{OZ} = 0.13$ nm^{-1}. Using the definition of ξ from the RPA and FH theories (see Appendix B), we can estimate the corresponding reduced segregation power ϵ to be about 0.036 (see eq B2). As this value is clearly smaller than unity, we can conclude the homogenized state corresponds to the single-phase state near the critical point, as in the case reported by Hashimoto et al.[38]

According to the scattering theory we do not expect a scattering maximum for the scattering profile for the homogenized state, simply because the scattering should be given by eq 15. The FFT pattern of the TEM images obtained from the sample immediately after 30 folding steps, however, shows a very wide maximum or shoulder (curve 1 in Figure 9). This maximum corresponds to a domain spacing of 78 nm. The phase separation after reaching the single-phase state is very fast. As we need some time for the sample preparation (see above), especially in the fixation process by the staining agent, the structure observed on Figure 4a might not

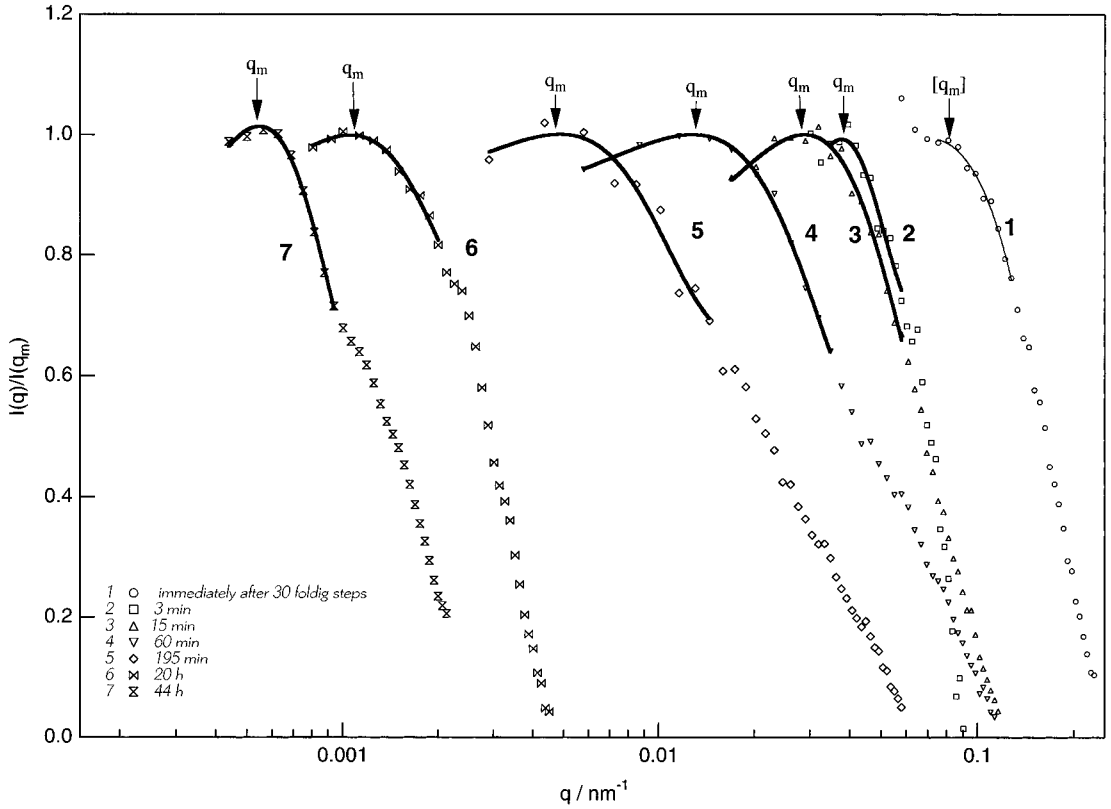

Figure 9. Plot of $I(q)/I(q_m)$ vs q of the circularly averaged power spectra obtained by 2D-FFT of the TEM (curves 1−5) and LSCM images (curves 6, 7) of the *near-critical* mixture (47 vol % SBR) at different stages of the annealing procedure at 100 °C. The spectra were obtained by averaging the spectra of (5) low-magnification images, respectively.

represent the real single-phase state but a structure which developed during the staining procedure until it is finally cross-linked and fixed. The domain spacing of 78 nm or the corresponding wavenumber $q_{m,hom} = 8.12 \times 10^{-2}$ nm^{-1} determined by FFT seems to be a very reasonable value compared to $q_{m2} \equiv 2\pi/\xi_{OZ} = 0.13$ nm^{-1} determined from the OZ plot.

IV. Summary

A detailed morphological analysis combining real (TEM and LSCM) and reciprocal (light scattering) space analysis methods of a polymer blend showing spinodal decomposition is presented for the first time. The microscopic investigations covered the whole range of the phase separation process, covering early, intermediate, and late stages. With the TEM we can observe structures from nanometer scale to several micrometers. The LSCM allows us to image bigger structures up to nearly the millimeter scale. With the TRLS we can observe structures at real time and do not have to freeze and fix the sample at different stages of the phase separation, but it is restricted to the observation in a small q-limit, smaller than $q_{max} \approx 10 \times 10^{-3}$ nm^{-1}, so that especially very small structures such as those expected during the early stage are not directly observable.

The SBR/PB blend having a near-critical composition shows a bicontinuous spongelike structure which appears immediately after the onset of the phase separation. During early, intermediate, and late stages, this bicontinuous structure keeps on growing as visible on the TEM and LSCM. During the growth period where microscopic methods and TRLS share a common observation window, the domain spacing measured by TRLS and the domain spacing observed on the microscopic images are in excellent agreement.

The structural evolution during the early stage was observed by TEM and subsequent 2D-FFT analysis on samples frozen by the OsO_4 fixation technique. The early stage of SD occurred in a very short time scale (at longest up to 10 min at 100 °C). The discrepancy between TEM/FFT and TRLS results can be possibly explained by an extrapolation error as described in the text, on applying Cahn's theory to the light scattering data.

Acknowledgment. The authors would like to thank the Japan Society for Promotion of Science (JSPS), the Alexander von Humboldt Foundation, and the Ministry of Education, Science, Culture and Sports, Japan (Grant-in-Aid for Scientific Research on Priority Areas "Cooperative Phenomena in Complex Liquids" No. 07651106) for financial support.

Appendix A

The determination of q_m of the power spectra obtained from the TEM or LSCM images was done as follows: At first 2D-power spectra are calculated from the TEM and LSCM images. These spectra are circularly averaged, and a plot of the intensity (au) vs distance from the center of the power spectrum (in pixel^{-1}) is obtained. From this plot we obtain the position of the maximum δ_{FFT} (in pixel^{-1}) which has to be translated into a wavenumber q_m^{FFT} in nm^{-1}.

The relation between δ_{FFT} (in pixel^{-1}) and corresponding real space distance d_{real} (in pixel) is given by

$$d_{real} = 256/\delta_{FFT} \tag{A1}$$

The obtained value for d_{real} (in pixel) is then transferred into a real distance Λ_{real} (in nm) by considering the magnification of the microscopic image. The microscopic

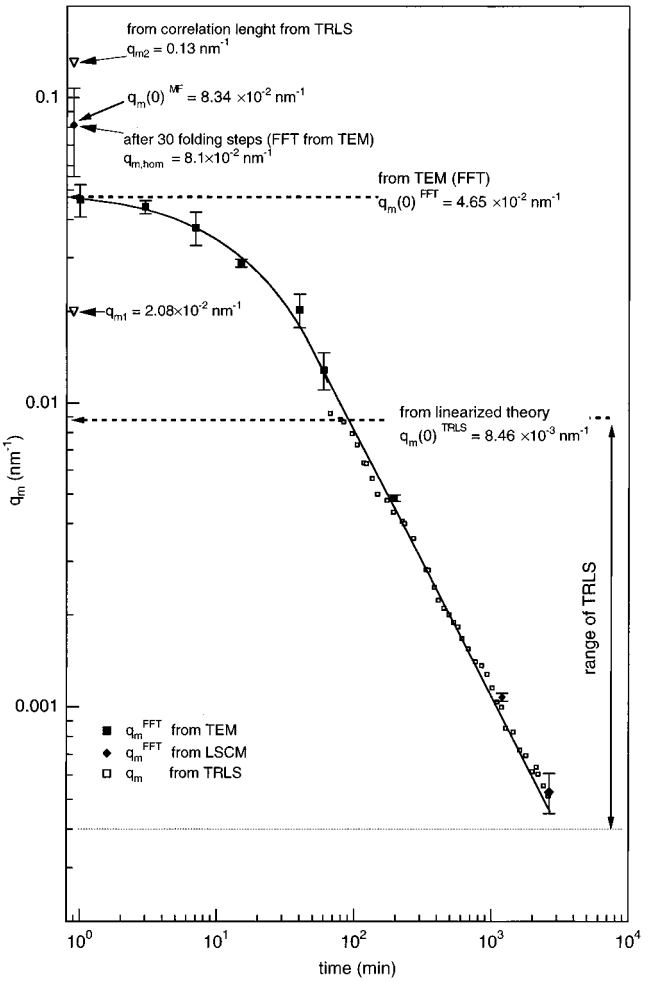

Figure 10. Combination of the data obtained by TRLS (□) and 2D-FFT (■ and ◆) on the time evolution of q_m during SD of the *near-critical* mixture (47 vol % SBR) annealed at 100 °C: $q_m(0)^{FFT} = 2\pi/\Lambda_m(0)^{FFT} = 2\pi/135$ nm^{-1} from the 2D-FFT and $q_m(0)^{TRLS} = 2\pi/\Lambda_m(0)^{TRLS} = 2\pi/740$ nm^{-1} from the TRLS with the linearized theory (doted arrows); $q_{m,hom} = 2\pi/\Lambda_{m,hom} = 2\pi/78$ nm^{-1} form the 2D-FFT of Figure 4a and $q_{m1} \equiv 1/\xi_{OZ} = 1/48$ nm^{-1} or $q_{m2} = 2\pi/\xi_{OZ} = 1/48$ nm^{-1} characterizing the homogenized state after 30 folding steps.

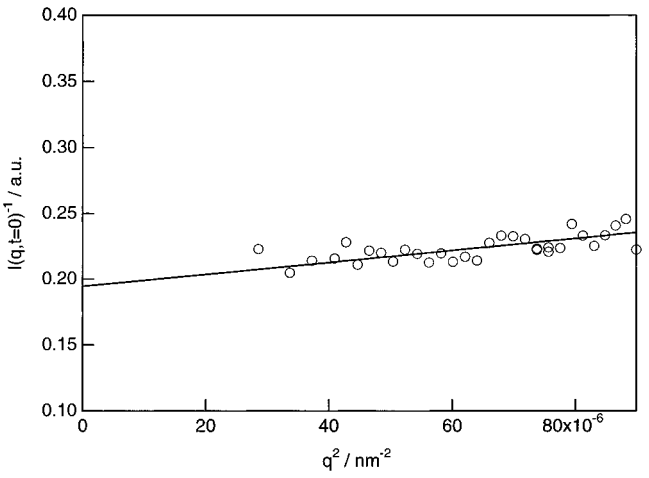

Figure 11. Ornstein−Zernike plot for the determination of ξ from the light scattering data immediately after homogenization.

images have a magnification which is known from the microscopic setup. The real distance obtained from the scale bars l_{sc} (in nm) of the respective images is converted into a pixel value d_{sc} (in pixel) by simply counting the pixels corresponding to the scale bar:

$$\Lambda_{real} = d_{real}(l_{sc}/d_{sc}) \quad \text{(A2)}$$

The obtained distance Λ_{real} is equal to the maximum of the domain spacing Λ_m^{FFT} and is finally recalculated into the corresponding wavenumber q_m^{FFT} using

$$\Lambda_m = 2\pi/q_m^{FFT} \quad \text{(A3)}$$

Appendix B

From the RPA, the thermal correlation length ξ in the single-phase mixture is given by

$$\xi^2 = \frac{a^2}{36\phi_{PB}(1-\phi_{SBR})(\chi_s - \chi)} = \frac{a^2}{36\phi_{PB}(1-\phi_{SBR})}\epsilon^{-1}\chi_s^{-1} \quad \text{(B1)}$$

with $\epsilon \equiv -\epsilon_T$, where ϵ_T is given by eq 5, i.e.,

$$\epsilon = [\chi_s - \chi(T)]/\chi_s \quad \text{(B2)}$$

From Flory−Huggins:

$$2\chi_s = \frac{1}{\phi_{PB}N_{PB}} + \frac{1}{(1-\phi_{SBR})N_{SBR}} \quad \text{(B3)}$$

Equations B1 and B3 give

$$\xi^2 = \frac{a^2 N_{PB}N_{SBR}}{18[\phi_{PB}N_{PB} + (1-\phi_{SBR})N_{SBR}]}\epsilon^{-1} \quad \text{(B4)}$$

From the OZ plot (Figure 11), we determined ξ to be 48 nm. Together with the statistical segment length $a_{PB} = 0.69$ nm for PB, obtained from literature data,[54] and assuming that $a_{PB} \cong a_{SBR} \cong a$, we calculate ϵ to be 0.0359. Thus the homogenized state is a single-phase state close to the critical point.

References and Notes

(1) Cahn, J. W. *J. Chem. Phys.* **1965**, *42*, 93.
(2) Hashimoto, T.; Kumaki, J.; Kawai, H. *Macromolecules* **1983**, *16*, 541.
(3) Snyder, H. L.; Meakin, P. *J. Chem. Phys.* **1983**, *79*, 5588.
(4) Hashimoto, T. *Phase Transitions* **1988**, *12*, 47. Hashimoto, T. In *Materials Science and Technology, Vol.12: Structure and Properties of Polymers*; Thomas, E. L., Ed.; VCH: Weinheim, 1993; Chapter 6.
(5) Kuwahara, N.; Sato, H.; Kuboto, K. *J. Chem. Phys. Commun.* **1992**, *97* (8), 5905.
(6) Bates, F. J.; Wiltzius, P. *J. Chem. Phys.* **1989**, *92*, 3208.
(7) Higgins, J. S.; Fruitwala, H. A.; Tomlins, P. E. *Br. Poym. J.* **1989**, *21*, 247. Higgins, J. S.; Fruitwala, H. A.; Tomlins, P. E. *Macromolecules* **1989**, *22*, 3674.
(8) Jinnai, H.; Hasegawa, H.; Hashimoto, T.; Han, C. C. *Macromolecules* **1991**, *24*, 282. Jinnai, H.; Hasegawa, H.; Hashimoto, T.; Han, C. C. *J. Chem. Phys.* **1993**, *99*, 4845, 8154. Hashimoto, T.; Jinnai, H.; Hasegawa, H.; Han, C. C. *Physica A* **1994**, *204*, 261.
(9) Nishi, T.; Wang, T. T.; Kwei, T. K. *Macromolecules* **1975**, *8*, 227.
(10) Laeuger, J.; Lay, R.; Gronski, W. *J. Chem. Phys. Lett.* **1994**, *78*, 1018.
(11) Lauger, J.; Lay, R.; Maas, S.; Gronski, W. *Macromolecules* **1995**, *28*, 7010.
(12) Jinnai, H.; Nishikawa, N.; Koga, T.; Hashimoto, T. *Macromolecules* **1995**, *28*, 4782.
(13) Ribbe, A.; Jinnai, H.; Hashimoto, T. *J. Mater. Sci.* **1996**, *31*, 5837.
(14) Jinnai, H.; Yoshida, H.; Kimishima, K.; Funaki, Y.; Ribbe, A.; Hashimoto, T. *Macromolecules* **1996**, submitted for publication.
(15) Voigt-Martin, G. J.; Leistner, K. H.; Rosenau, R.; Koningsveld,

R. *J. Polym. Sci., Polym. Phys. Ed.* **1986**, *24*, 723.
(16) Shabana, H.; Guo, W.; Olley, R. H.; Basset, D. C. *Polym. Commun.* **1993**, *34* (6), 1313.
(17) Tao, J.; Okada, M.; Nose, T.; Chiba, T. *Polymer* **1995**, *36*, 3909.
(18) Ribbe, A.; Hashimoto, T. *Proceedings of the Bayreuth Polymer Symposium*, Bayreuth, Germany, 1995; pp 82−85.
(19) Kim, B. S.; Chiba, T.; Inoue, T. *Polymer* **1995**, *36* (1), 43.
(20) Gunton, J. D.; San Miguel, M.; Sahni, P. S. In *Phase Transition and Critical Phenomena*; Domb, C., Lebowitz, J. L., Eds.; Academic Press: New York, 1983; Vol. 8, p 269.
(21) Shinozaki, A.; Oono, Y. *Phys. Rev. Lett.* **1991**, *66*, 173.
(22) Koga, T., Kawasaki, K. *Phys. Rev.* **1991**, *A44*, 817.
(23) Koga, T., Kawasaki, K. *Physica A* **1993**, *196*, 389.
(24) Takenaka, A.; Hashimoto, T. *Phys. Rev. E, Rapid Commun.* **1993**, *48* (2), 647.
(25) Izumitani, T.; Hashimoto, T. *J. Chem. Phys.* **1985**, *83*, 3694.
(26) Takenaka, M.; Izumitani, T.; Hashimoto, T. *Macromolecules* **1987**, *20*, 2257.
(27) Izumitani, T.; Takenaka, M.; Hashimoto, T. *J. Chem. Phys.* **1990**, *92*, 3213.
(28) Takenaka, M.; Izumitani, T.; Hashimoto, T. *J. Chem. Phys.* **1990**, *92*, 4566.
(29) Takenaka, M.; Izumitani, T.; Hashimoto, T. *J. Chem. Phys.* **1993**, *98*, 3528.
(30) de Gennes, P. G. *J. Chem. Phys.* **1980**, *72*, 4756.
(31) Pincus, P. *J. Chem. Phys.* **1981**, *75*, 1996.
(32) Binder, K. *J. Chem. Phys.* **1983**, *79*, 6387.
(33) Langer, J. S.; Baron, M.; Miller, H. D. *Phys. Rev.* **1975**, *A11*, 1417.
(34) Hashimoto, T.; Takenaka, M.; Jinnai, H. *J. Appl. Crystallogr.* **1991**, *24*, 457.
(35) Takenaka, M.; Hashimoto, T. *J. Chem. Phys.* **1992**, *96*, 6177.
(36) Jinnai, H.; Hashimoto, T.; Lee, D.; Chen, S. H. *Macromolecules* **1997**, *30*, 130.
(37) Hashimoto, T.; Jinnai, H.; Nishikawa, Y.; Koga, T.; Takenaka, H. *Progr. Colloid Polym. Sci.* **1997**, in press.
(38) Hashimoto, T.; Izumitani, T.; Takenaka, M. *Macromolecules* **1989**, *22*, 2293.
(39) Ribbe, A.; Hashimoto, T. *Macromolecules*, to be submitted.
(40) Wilson, T. *Confocal Microscopy*; Academic Press: London, 1990. Product specification ZEISS LSM 320.
(41) Ribbe, A.; Hayashi, M.; Hashimoto, T. *Macromolecules*, to be submitted.
(42) Hashimoto, T.; Itakura, M.; Shimidzu, N. *J. Chem. Phys.* **1986**, *85*, 6773.
(43) Binder, K.; Stauffer, D. *Phys. Rev. Lett.* **1974**, *33*, 1006.
(44) Hashimoto, T.; Itakura, M.; Hasegawa, H. *J. Chem. Phys.* **1986**, *85*, 6118.
(45) Kawasaki, *K. Progr. Theor. Phys.* **1977**, *57*, 826. Kawasaki, K.; Ohta, T. *Progr. Theor. Phys.* **1978**, *59*, 362.
(46) Jinnai, H.; Koga, T.; Nishikawa, Y.; Hashimoto, T.; Hyde, S. T. *Phys. Rev. Lett.* **1997**, *78*, 2248.
(47) Jinnai, H.; Nishikawa, Y.; Hashimoto, T. *Polym. Prepr. Soc. Polym. Sci. Jpn.* **1994**, *43* (9), 2899.
(48) Cahn, J. W.; Hilliard, J. E. *J. Chem. Phys.* **1959**, *32*, 688.
(49) Cook, H. E. *Acta Metall.* **1970**, *18*, 297.
(50) Strobl, G. R. *Macromolecules* **1985**, *18*, 558.
(51) Okada, M.; Han, C. C. *J. Chem. Phys.* **1986**, *85*, 5317.
(52) Ornstein, L. S.; Zernike, F. *Proc. Akad. Sci. Amsterdam* **1914**, *17*, 793.
(53) Tanaka, H.; Hayashi, T.; Nishi, T. *J. Appl. Phys.* **1986**, *59*, 3627.
(54) Brandrup, J., Immergut, E. H., Eds. *Polymer Handbook*; Wiley: New York, 1975.

MA970258I